Journal of Materials Chemistry

Cite this: J. Mater. Chem., 2011, 21, 14622

www.rsc.org/materials

PAPER

Nano-scale chemical imaging of a single sheet of reduced graphene oxide

J. G. Zhou,*[a] J. Wang,*[a] C. L. Sun,[b] J. M. Maley,[c] R. Sammynaiken,[c] T. K. Sham*[d] and W. F. Pong[e]

Received 11th March 2011, Accepted 14th June 2011
DOI: 10.1039/c1jm11071c

Scanning transmission X-ray microscopy (STXM) has been used to chemically image single and multiple layers of a thermally reduced graphene oxide (r-GO) multi-layer sheet of the size of ~1 μm and a thickness of ~5 nm. The thickness of individual layers in the single sheet can be identified through quantitative analysis of STXM. The local electronic and chemical structure of interest (edge *versus* center) in different regions within the single r-GO sheet has been studied by C K-edge X-ray absorption near edge structure spectroscopy (XANES) with 30 nm spatial resolution. High and localized unoccupied densities of states (DOS) of carbon σ* character were observed in r-GO compared to graphite and were interpreted as the lack of strong layer to layer interaction in the former. The azimuthal dependence of C K-edge XANES in selected locations has also been obtained and was used to infer the preferred edge structure. The r-GO sample was also characterized by TEM, AFM and Raman spectroscopy; the findings are in good accord with the STXM results.

1. Introduction

Graphene, a single atomic plane of graphite, has quickly elevated as a star in materials science and condensed-matter physics since its discovery in 2004[1] due to its outstanding and very unique electronic, chemical and mechanical properties.[2–4] While chemical avenues such as epitaxial growth[5] and exfoliation of functionalized graphite[6,7] are suitable for making this unique 2D material in large scale, historically, mechanical cleavage of a 3D graphite flake was the main route.[2] Exfoliation of graphite is commonly carried out using a modified Hummer method, which involves the oxidation of graphite followed by sonication.[6,7] The resulting product of this method is often called graphene oxide (GO), which is electronically insulated due to the disruption of the crystallinity by the introduction of surface functional groups (particularly epoxide and carboxylic). GO has an inter-planar separation considerably larger than that of graphite.[8,9] Reduction of GO (r-GO) by the hydrothermal method,[10] annealing under various environments[9] or chemical reduction[11] can restore the conductivity to some extent. GO and r-GO or doped r-GO have been widely used in energy storage,[10,12] catalysis[13] and electronic devices[9,14,15] either as a support or as an active material with superior properties. The morphology of nanocrystalline adsorbates on r-GO surfaces can be tuned through adjusting the surface functional group in GO, which serves as an "anchoring site".[6] Such an anchoring event is believed to provide a good connection between coated catalyst nanocrystals and the GO support, leading to desirable properties in such nanocomposites.[10,12] The interaction in carbon nanotube (CNT) based nanocomposites and its effect on catalyst performance have been studied previously.[16–19] Although the CNT can be envisioned as rolled multi-layer graphene sheets, which possesses desirable properties as catalyst support, it has been found that the r-GO supported catalyst has in fact much enhanced catalytic capability over the CNT support.[13,20] This enhanced performance must be related to the r-GO's unique electronic structure, although experimental evidence is still relatively lacking.

X-ray absorption near edge structure spectroscopy (XANES) is a powerful method for studying the local structure (electronic and chemical structure) of nanomaterials.[16,18,19,21–28] XANES at the C K-edge is concerned with the measurement and interpretation of the absorption coefficient associated with the excitation of the C 1s electron to previously unoccupied electronic states as the photon energy is scanned across the excitation threshold. The unoccupied states can be (i) bound states (below the ionization threshold, *i.e.* the vacuum level) such as the π* lowest unoccupied molecular orbital (LUMO) in benzene or graphite; the orientation of the molecular orbital (axis) of the π* orbital in benzene for example is perpendicular to the basal plane, (ii) quasi-bound, potential barrier states (above the vacuum level but trapped by a potential barrier set up by surrounding atoms), such as the σ* orbitals in benzene whose orientation is in the basal plane and is sometimes referred to as multiple scattering states, and (iii) the continuum (photoelectrons leaving the system). These transitions are dominantly

[a]*Canadian Light Source Inc., University of Saskatchewan, Saskatoon, Canada S7N 0X4. E-mail: jigang.zhou@lightsource.ca; jian.wang@lightsource.ca*
[b]*Department of Chemical and Materials Engineering, Chang Gung University, Tao-Yuan, Taiwan*
[c]*Saskatchewan Structural Sciences Centre, University of Saskatchewan, Canada*
[d]*Department of Chemistry, University of Western Ontario, London, Canada N6A 5B7. E-mail: tsham@uwo.ca*
[e]*Department of Physics, Tamkang University, Tamsui, 251, Taiwan*

dipolar, therefore, C 1s excitation probes the unoccupied electronic states of C 2p character. The nature of the bound and quasi-bound states is strongly influenced by the neighbouring atoms (coordination number, symmetry and bonding). The position and relative intensity of these resonances can be used to infer the structure and bonding of the sample under investigation. Furthermore, tunable polarization achievable from the Elliptically Polarized Undulator (EPU) on the SM beamline at the Canadian Light Source employed in this experiment permits the selection of linear and circular polarization.[29] Linear polarization can be used to determine the orientation of the molecular framework by orientating the polarization vector of the incident light at various angles with respect to the orientation of the sample and observe the relative intensity of the π* and σ* resonances, which is proportional to the transition matrix element, $|\langle i|\boldsymbol{e}\cdot\boldsymbol{r}|f\rangle|^2 \propto |\langle i|\cos\theta|f\rangle|^2$ where $\langle i|$ and $|f\rangle$ represent initial and final states, $\boldsymbol{e}$ and $\boldsymbol{r}$ the polarization vector and the electron coordinate, respectively, θ the angle between the polarization and the orientation of the π* and σ* orbitals for example. Circular polarized light can be used to eliminate linear dichroism in chemical imaging.

Several XANES studies of GO or r-GO and graphene prepared by chemical vapour deposition have been reported[5,8,11,30,31] along with electronic structure calculations.[32,33] These studies show generally their graphitic-like feature and the presence of oxygen containing functional groups. They all exhibit a sharp π* transition at ~285.5 eV and a σ* resonance at ~291 eV followed by progressively broader σ* type resonances. What is unique for graphene however is the existence of a singularity at 283–284 eV, often referred to as a defect peak. This peak was first reported by Pereira *et al.*[27] and later on by others. This defect peak is absent in highly ordered pyrolytic graphite (HOPG) but appears after controlled ion beam doping with C^+ and is attributed to defects created by ion bombardment.[34] Conventional XANES is conducted over a sampling area significantly larger than the size of an individual nanostructure so that it probes the average property. Thus, the structure variation between GO and r-GO sheets and variation within a single sheet cannot be obtained, and furthermore, impurities, which are often present albeit in small amount, also contribute to the signal. These are drawbacks of techniques with a large probing area for studying nanomaterials in general and graphene (including GO and r-GO) in particular since it is well accepted that the edge structure of graphene, namely "armchair" and "zigzag", is crucial for its performance[9,14] and high spatial resolution is required to study them. Another challenge using conventional XANES in studying shallow core levels is that quantitative information on absorption, hence the sample thickness, cannot be readily obtained using the yield detection modes (electron yield or X-ray fluorescence yield), which is often used since the absorption length in this energy range, *e.g.* C K-edge, is very short (~100 nm) and an ultrathin uniform specimen required for transmission measurements in conventional XANES is difficult to prepare. Scanning transmission X-ray microscopy (STXM) using a focused beam of the size of nm provides an excellent combination of chemical/electronic structure speciation (XANES) and microscopy studies of a small single sheet of r-GO on the order of nm thick and hundreds of nm wide. The SM beamline at the Canadian Light Source provides STXM capability with a spatial resolution of 30 nm and a spectral resolution of better than 0.05 eV.[29] It has been successfully applied to studies of the electronic structure and surface interaction of an individual CNT supported catalyst[17,35] as well as dopant distribution in a single N-doped CNT.[36] This study reports an application of STXM in the chemical imaging of a single r-GO sheet with varying thickness (containing several layers). The electronic and chemical structure of selected regions (thin edge, a single layer and thicker center, multi-layers) within this sheet is obtained by XANES at C K-edges in transmission. Such information will advance our understanding of the electronic structure of r-GO, especially as a building block in nanocomposites.

2. Experimental

GO was made following the modified Hummers' method,[37] then reduced to r-GO through annealing at 1050 °C under a low pressure, argon gas flow environment. Briefly, commercial natural graphite powder (from Alfa Aesar) was used as the starting material. Graphite (5 g) was first mixed with sulfuric acid (87.5 mL) and nitric acid (45 mL) and stirred. Potassium chlorate (55 g) was then added slowly and stirred for over 96 hours; after that graphene oxide (GO) powder was obtained. The GO was rinsed repeatedly in a 5% solution of HCl then washed with deionized water several times. Finally, the GO was heated to 1050 °C under vacuum with 2 Torr argon gas flow and held at this temperature in the furnace to form the reduced graphene oxide (r-GO).

r-GO powder was dispersed in ethanol by sonication, then deposited on porous lacey carbon film coated TEM grids for transmission electron microscopy (TEM) and STXM measurements, and deposited on Si_3N_4 windows (thickness 100 nm, Norcada Inc.) for atomic force microscopy (AFM) and Raman spectroscopy measurements. TEM was carried out on a Jeol JEM-1230 operating at 100 kV. AFM was conducted on an Agilent 4500 AFM in intermittent contact mode using a silicon cantilever (Nanoscience Instruments) with a curvature of radius of <10 nm, a force constant of approximately 48 N m^{-1}, and a resonant frequency of approximately 190 kHz. The AFM scan rate was set to be 0.5–1.0 Hz (512 pixels per line) for all images. Raman spectroscopy measurements were carried out on a Renishaw InVia Reflex Raman microscope using an argon-ion laser (Spectra-Physics Model 153-M42-010) operating at 514.5 nm, and an 1800 lines per mm grating. The microscope was focused onto the sample with a 100× N PLAN objective lens (NA = 0.85), and Raman spectra were obtained using the Streamline line focus mode with a 10 s detector exposure time. The laser power was 0.23 mW measured at the sample. The instrument calibration was verified using an internal Si sample at 520 cm^{-1}.

STXM measurements were conducted using the STXM at the SM beamline of the Canadian Light Source (CLS), a 2.9 GeV third generation synchrotron facility. The SM STXM is equipped with a 25 nm outermost-zone zone plate (CXRO, Berkeley Lab), and the diffraction-limited spatial resolution for this zone plate is 30 nm. A 250 line mm^{-1} plane grating monochromator (PGM) was used for C K-edge measurements. The incident photon flux (I_o) count rate was tuned to be ~20 MHz as read by the STXM detector in a hole of the STXM sample plate at 320 eV with exit slits at 35/35 μm (dispersive/non-dispersive). The C K-edge image stacks covered an energy range of 280–320 eV with an energy step

as fine as 0.1 eV around the XANES peaks and coarser, 0.4–1.0 eV, in the pre-edge and continuum. The image pixel size was 25 nm with 1 ms dwell time per pixel. X-ray photon energy was calibrated using the gas phase XANES of CO_2 reported in the literature.[38] Circularly and linearly polarized soft X-ray beam generated from the SM EPU was used as appropriate. The use of circular polarized light averages out the in-plane polarization dependence of the absorption. Two sample orientations were used: first, the photon beam is incident normal to the sample surface so that the electric polarization lies on the surface basal plane and second, the incident beam was at a 30 degree angle of incidence relative to normal. The in-plane azimuthal polarization dependence of C K-edge XANES was performed using linear polarization (normal incidence) adjusted to be parallel, perpendicular, 30°, and −30° with respect to the edge of the r-GO sheet of interest.

STXM data were analyzed by aXis2000 (available free for non-commercial applications at http://unicorn.mcmaster.ca/aXis2000.html). The C K-edge XANES from interesting locations were extracted from image stacks using image masks which allow only selection of the regions of interest. XANES spectra from pure r-GO, lacey carbon and impurity regions were used as reference spectra with the r-GO spectrum further quantitatively scaled for image stack fitting to generate chemical component maps. The color composite map was created by combining individual component maps with the image intensity rescaled for better visualization. More details of STXM experimental and data analysis procedures can be found elsewhere.[17,36]

3. Results and discussions

3.1 Characterization of the r-GO sample by laboratory techniques

Fig. 1 presents the characterization results of the r-GO sample using TEM, AFM and Raman spectroscopy. The TEM image in Fig. 1a shows the multi-layered general morphology of the r-GO sheet that was used in this study. It also indicates the possibility of folding the r-GO sheet to form thicker regions. Fig. 1b shows an AFM topography image of the r-GO sample showing some small isolated sheets. The Z_{mean} of these sheets was 5.5 ± 1.8 nm

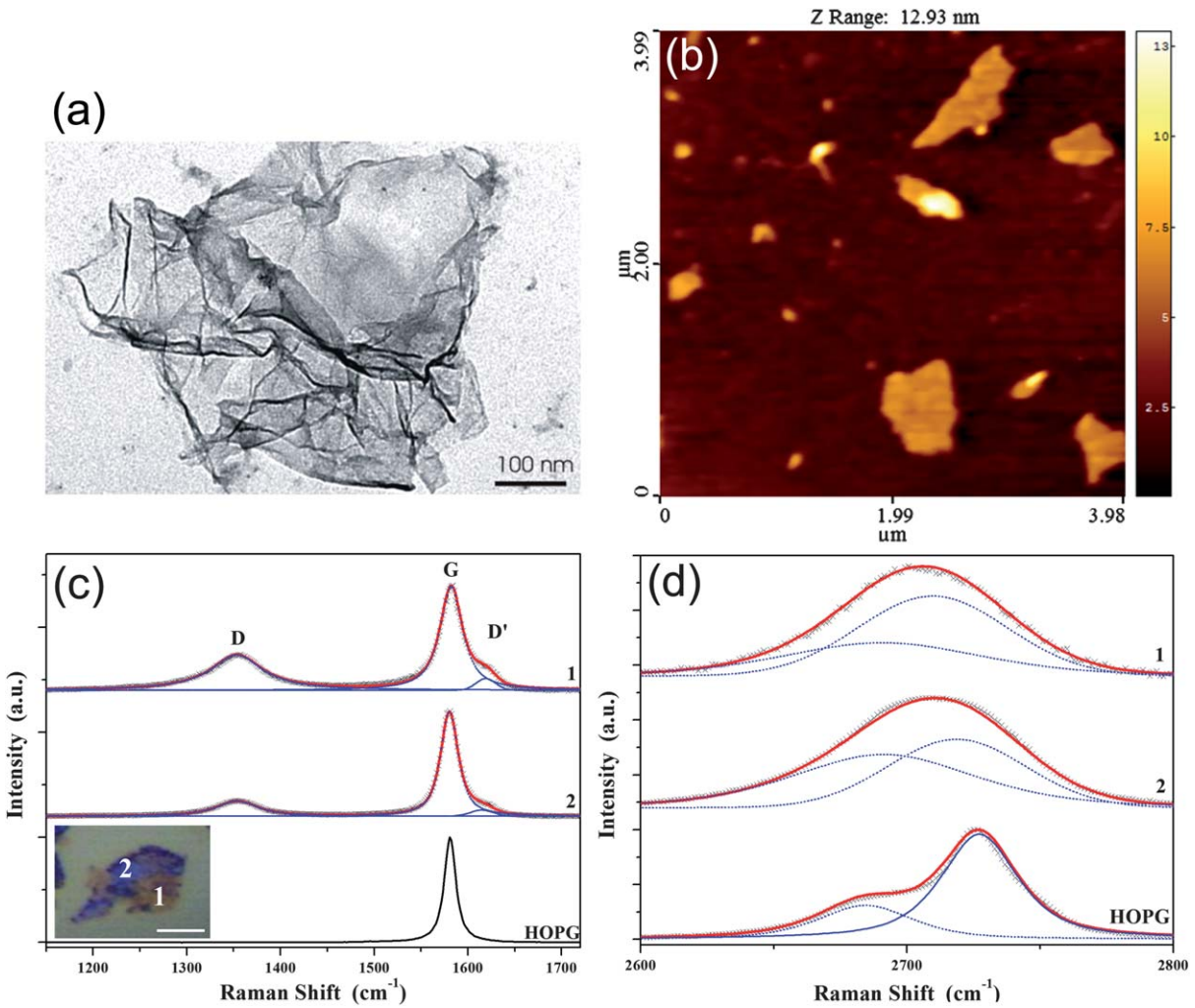

Fig. 1 Characterization of the r-GO sample by TEM, AFM and Raman spectroscopy: (a) TEM image of r-GO; (b) AFM topography image of isolated r-GO sheets (the Z_{mean} of the sheets was 5.5 ± 1.8 nm thick); (c) Raman spectra of the D′, G and D bands of a r-GO sheet taken at two spots and the HOPG (the inset optical image shows the r-GO sheet and the two spots for Raman spectroscopy measurements, the scale bar is 5 μm); (d) Raman spectra of the 2D band of the r-GO sheet taken at two spots and the HOPG.

Table 1 Peak fitting analysis of the Raman spectra of a single r-GO sheet taken at two spots and the HOPG[a]

	2D band/cm^{-1}						
Sample	Peaks		Difference/cm^{-1}	D′ band/cm^{-1}	G band/cm^{-1}	D band/cm^{-1}	I_D/I_G
r-GO spot 1	2691 (88)	2710 (66)	19	1619 (25)	1582 (29)	1353 (68)	0.34
r-GO spot 2	2691 (88)	2719 (66)	28	1615 (29)	1580 (23)	1354 (54)	0.14
HOPG	2684 (42)	2727 (34)	43	—	1580	—	0

[a] *N.B.*: FWHM values are given in brackets.

averaged from 13 isolated sheets, and the $Z_{\text{std. dev.}}$ (surface height variation of the isolated sheets) was 1.6 ± 0.6 nm. Fig. 1c and d present the Raman spectra of a single r-GO sheet taken at two locations on the sheet compared with the HOPG standard sample. The inset of Fig. 1c shows an optical image of the r-GO sheet and the two spots (labelled 1 and 2 in white color) for Raman spectroscopy. In Fig. 1c three main peaks are found in the 1200–1700 cm^{-1} range. The G band (~1580 cm^{-1}) is associated with the E_{2g} phonon mode. The D band (~1350 cm^{-1}) is associated with disorder induced defects. If sufficient amount of defects are present in the sample, a second defect band called the D′ band (~1620 cm^{-1}) may appear. Spot 2 shows much less intensity on the D′ band and darker color in the optical image than spot 1, which suggests that spot 2 has higher crystalline order. It has been well established that the shape of the 2D band around 2700 cm^{-1} in Raman spectroscopy is very sensitive to the number of graphene layers.[39] In graphene samples, the splitting between the two main peaks under the 2D band increases with increasing graphene layers approaching the bulk value associated with HOPG.[40] The peak fitting result of the Raman spectra of the two spots on the r-GO sheet and the HOPG is listed in Table 1, from which it shows that spot 1 has a 2D band splitting of 19 cm^{-1} smaller than 28 cm^{-1} of spot 2, thus the spot 1 region is thinner. Furthermore the splitting at spot 1 is very close to the bilayer graphene splitting of ~20 cm^{-1} reported in the literature,[39] suggesting that the isolated r-GO sheet can be as thin as the bilayer.

3.2 Chemical imaging of a single r-GO sheet by STXM

STXM data of an r-GO sheet deposited on a lacey TEM grid at the C K-edge were collected with a circularly polarized X-ray beam perpendicular to the sample surface. The circular polarization study can avoid the possible linear dichroism effect due to crystalline orientation.[36,41] The chemical mapping of the r-GO sheet, lacey carbon substrate and impurities was performed by fitting the C K-edge STXM image stack with internal reference spectra of r-GO, lacey carbon and impurity (fitting of the image stack using only r-GO and lacey carbon generates a residue which was denoted as the impurity, and spectroscopically it mostly resembles aliphatic organics although aromatic or carbonyl functional group cannot be ruled out). Regardless of the origin, the overall contribution of the impurity to the signal is small. The impurity is akin to mechanically exfoliated graphene where the contamination was speculated to be hydrocarbon.[42] The r-GO reference spectrum was normalized to its 1 nm thick elemental absorption profile (assuming the density is 2.16 g cm^{-3}, same as graphite) by fitting at both 280 and 320 eV to represent a spectrum of 1 nm thickness r-GO. The 1 nm thick r-GO reference spectrum is still in optical density (OD) or absorbance (μt, where μ is the linear absorption coefficient and t the thickness), therefore the thickness of the r-GO sample can be mapped quantitatively based on it. The individual component and colour composite map of a piece of a single sheet of the r-GO sample (containing multilayers) is displayed in Fig. 2. The maximum thickness of the r-GO sheet is 3.2 nm after the removal of the contribution from the background as displayed in Fig. 2a. The image of the porous lacey carbon framework support is shown in Fig. 2b. Impurities were localized and concentrated on two regions on the r-GO sheet, as shown in Fig. 2c and d. Although impurity has been mapped in this study, its concentration actually is very low (as seen by the noisy spectrum in the inset of Fig. 2c); consequently its contribution to the electronic and chemical structure of r-GO is negligible. The ability to distinguish between different types of carbon (r-GO, lacey carbon and trace impurity) by STXM allows for the study of area-selected XANES spectroscopy on locations of interest, for example, single and multiple layers of r-GO and its edges.

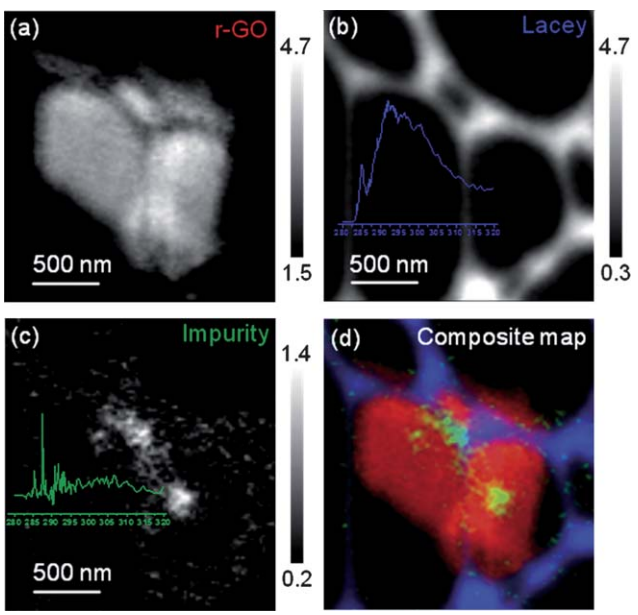

Fig. 2 Chemical mapping of a single multilayer r-GO sheet on lacey carbon: (a) r-GO, the vertical grey scale represents the thickness in nm; (b) lacey carbon, the corresponding C K-edge reference XANES is shown in the inset; (c) impurity, the C K-edge reference XANES spectrum is shown in the inset, the vertical grey scales of (b) and (c) represent the intensity ratio to the reference spectra; (d) colour composite map, red: r-GO, blue: lacey carbon, and green: impurity.

To illustrate further the thickness variation, especially the identification of the edges of stepping layers in r-GO, Fig. 2a is redisplayed by a 4-color contour map in Fig. 3a (green: 1.5–2.2 nm corresponding to X-ray absorption of ~1 layer r-GO, blue: 2.2–3.3 nm (absorption of 2 layers), red: 3.3–4.4 nm (absorption of 3 layers), and purple: 4.4–4.7 nm (absorption of 4 layers)). This quantitation takes into account that one layer of the graphene sheet is about 1.1 nm[43] or close to it as often observed experimentally.[44] Thus the discrete increment of 1.1 nm from one to four layers within the r-GO sheet strongly indicates that this sheet contains single and multilayers. This result is consistent with our AFM and Raman spectroscopy results. Fig. 3a also clearly reveals the edge in each layer and allows for further locating regions of interest for electronic structure and chemistry study.

3.3 C K-edge XANES of the entire single sheet of r-GO

The C K-edge XANES of the whole r-GO sheet with the X-ray beam (circular polarization) incident perpendicular to the basal plane of r-GO is shown in Fig. 3b, red curve, which was obtained through averaging XANES of all pixels except the impurity regions. The lack of π^* resonance intensity is apparent and this is due to the polarization effect in that the electric vector of the X-ray beam is lying on the plane, perpendicular to the π^* orbital. The spectral features at 283.7 eV and 285.4 eV, corresponding to the graphene defect and π^* resonance, respectively, are still observable albeit with very low intensity. The 283.7 eV feature is characteristic of single- or bi-layer graphene features due to defects as reported in the literature,[45] and the 285.4 eV peak arises from regions that are not perfectly flat due to the presence of non-aromatic regions in r-GO or wrinkle/folding of the sheet. In addition, r-GO is known to contain many crystalline domains surrounded by areas of defects within a single sheet. The presence of these domains in our specimen is supported by the appearance of D (~1350 cm^{-1}) and G (~1580 cm^{-1}) bands in the Raman spectrum. The intensity ratios of D/G band (see Table 1) show that the dimension of the crystalline domain in the r-GO sheet is about 300–700 nm.[46] To prove that the absence of π^* resonance in the normal incident geometry is due to the polarization effect as stated above and the sheet is nearly flat, the polarization effect

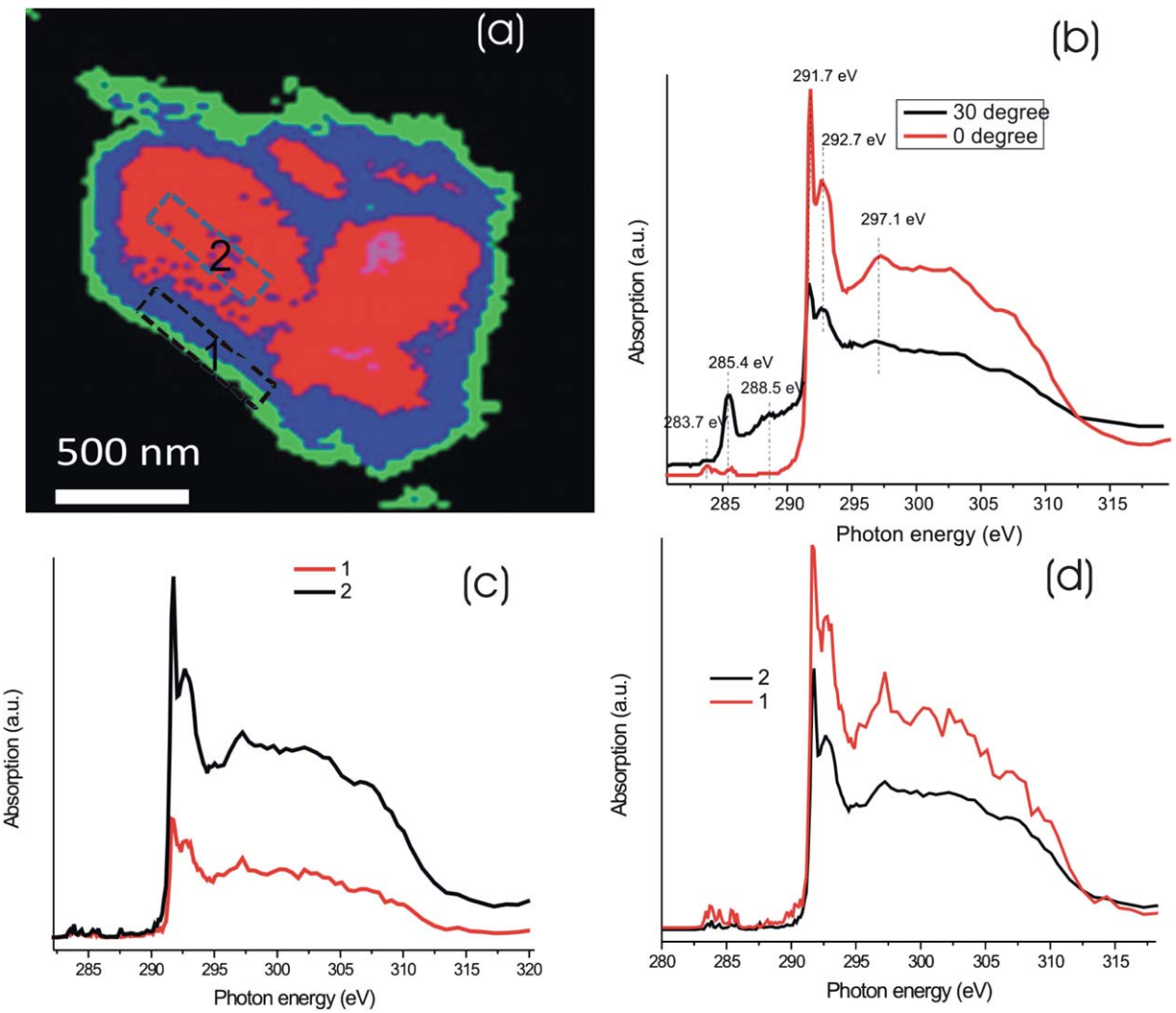

Fig. 3 (a) Multiple layer mapping of the single multilayer r-GO sheet; (b) angle dependent C K-edge XANES of the entire sheet (averaged over all pixels except impurity contributions); (c and d): C K-edge XANES for regions 1 and 2 (normal incidence) before and after normalization to absorption at 314 eV, respectively (the difference in the statistics is due to the fact that the OD of region 2 is about 3 times that of the OD of region 1 before normalization).

on C K-edge XANES was further examined at an incidence off normal (rotating the normal of the r-GO sheet by 30 degrees from the incident beam).

The C K-edge XANES, obtained again by averaging all pixels of the r-GO sheet at this angle, is displayed in Fig. 3b (black curve). As expected at this angle, we observe an increase in the intensity of the π* resonance at 285.4 eV accompanied by a decrease in intensity in the σ* resonance, as their orbital axes are orthogonal. Interestingly, we also observe a noticeable peak at 288.5 eV with increasing background, this peak can be attributed to the π* of the C═O moiety of the carboxylic group. Since this peak is absent in normal incidence (red curve), this observation indicates that such functional groups "lie" in the basal plane, therefore they are likely concentrated along the edge. The peak at 283.7 eV is less sensitive at this angle which means that it has little texture, consistent with randomly distributed site vacancy. O K-edge XANES at normal incidence was also recorded (not shown) and the signal is weak and very noisy indicating that the concentration of the oxygen containing group is very low in agreement with the C K-edge XANES discussed above. O K-edge XANES from other r-GO sheet shows that the oxygen functional group exhibits characteristics of a carboxyl group while an epoxide (rich in GO) feature is absent.[8]

3.4 Area selected C K-edge XANES: the central region *versus* the edge

The structure variation along selected regions was further investigated. Two regions were selected as shown in Fig. 3a (each region about 500 nm × 100 nm): region 1 is the thinnest (one and two layers) and covers an area including the edge of the sheet; region 2 is a thicker region (three to four layers) near the center of the sheet away from the edges. It should be noted that the C K-edge XANES (at normal incidence) of region 1 (red curve) has a smaller edge jump compared to that of region 2 (black curve) before normalization. This observation confirms that region 1 is thinner (see Fig. 3c). The XANES for these two regions after normalization to a unity edge jump at 314 eV are displayed in Fig. 3d (red curve for region 1 and black for region 2). As discussed above, region 1 exhibits more defect features as seen in the enhanced 283.7 eV resonance. Another observation is that the normalized intensity of σ* at 291.7 eV and multiple scattering peaks beyond show thickness dependence; *i.e.* it decreases in a thicker r-GO region. Since this normalized peak represents the unoccupied density of states with C 2p character and multiple scattering states as the photon energy increases beyond the first σ* at 291.7 eV, its variation reflects possible charge redistribution within different layers of the r-GO sheet and the reduction of multiple scattering pathways from other layers in the case of a single layer or bilayer (region 1). This is conceivable since a thicker r-GO (region 2) has a higher possibility for layer interaction (for instance, π–π interaction between r-GO layers) than a thin r-GO (region 1). Very interestingly, the thickness dependent σ* intensity variation is only observed in normal incident XANES where the absorption is at its maximum but not in the 30° XANES (Fig. 4 compared with Fig. 3b) where the sample is thicker. The comparison of C K-edge XANES between thin and thick r-GO in Fig. 4 also shows that the thin r-GO (containing the edge region) has a noticeably enhanced 283.7 eV feature and a weaker π* resonance (hence enhanced σ*/π*). This observation shows that there are rich defects in the edge region as discussed above. It has been shown that a CNT tip with rich defects exhibits significantly enhanced intensities of both π*- and σ*-band at C K-edge XANES.[47] Spectral features between π* and σ* (~288 to 289 eV) in both regions indicate the presence of oxygen containing groups such as a carboxyl group.

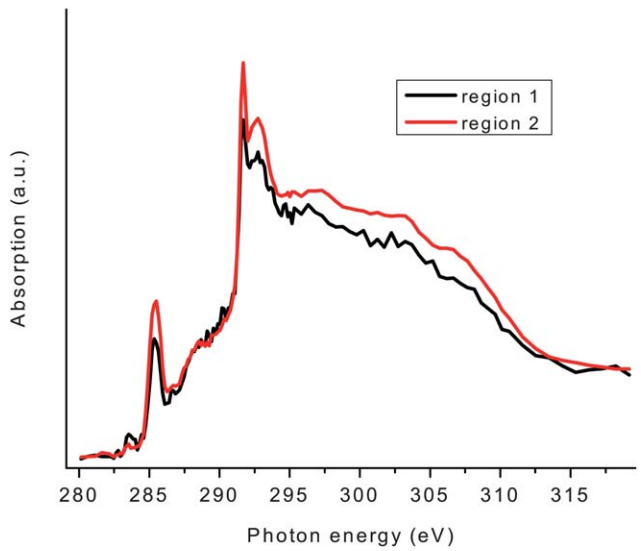

Fig. 4 C K-edge XANES of r-GO in regions 1 and 2 at 30 degree angle of incidence relative to normal.

To further check the origin of the enhanced absorption in thin r-GO, we compare normalized C K-edge XANES of multi-walled carbon nanotubes (MWCNTs)[17] to that of r-GO obtained at normal incident and at 30 degree incidence using STXM (Fig. 5a normalized at 315 eV, and Fig. 5b normalized at 300 eV). The MWCNTs show much reduced intensity in their characteristic π* and σ* resonances as well as the multiple scattering regions than that of r-GO. Assuming that there are no countervailing scattering and matrix element arguments, we attribute this to the lack of inter-planar interaction in r-GO which is strong in MWCNTs. Another observation is the very sharp and very intense 1st σ* (peak at 291.7 eV, also referred to as core exciton due to its long lifetime) relative to the 2nd σ* (peak at 292.7 eV) in r-GO (lifetime usually gets shorter as the kinetic energy of the photoelectron trapped in the potential well increases, hence the resonance gets broader). Such unusually sharp (localized) peak in r-GO clearly results from the lack of inter-planar interaction, and this is very likely why graphene plays a crucial role in strengthening the interaction with adsorbed metal in the r-GO supported catalyst, resulting in the enhanced catalytic capability of r-GO relative to the CNT support.[13,20]

The structural difference between region 1 and region 2 is further examined by the azimuthal linear polarization dependence of C K-edge XANES (Fig. 6) with the normal incident beam. Normalized 291.7 eV (1st σ*) and 292.7 eV (2nd σ*) intensity (measured by the height of the resonance, summarized in Table 2) at different polarizations is shown in Fig. 7. It again shows that the thinner region containing the edge of the r-GO layer presents a more obvious angle dependence which can be due to defects tiling from the basal plane as well as broken symmetry of the edge atoms. This azimuthal effect also may

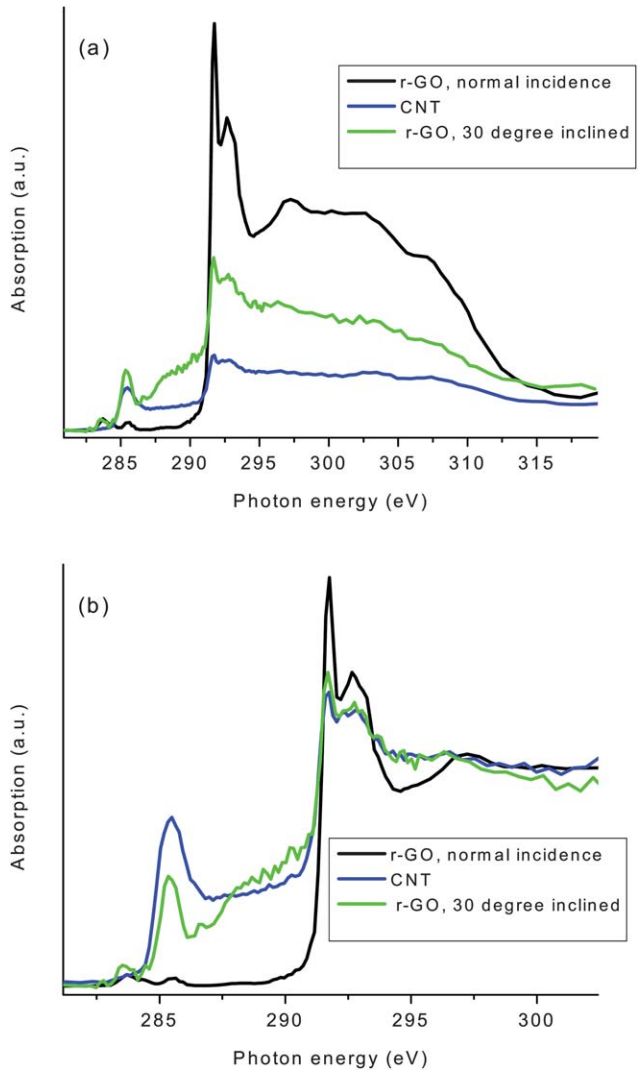

Fig. 5 (a) C K-edge XANES of r-GO (black curve) normal incidence, 30 degree incidence (green curve) of the edge region, and MWCNT (blue curve) normalized at 315 eV; (b) same spectra as presented in (a) but the spectra were normalized to unit jump at 300 eV instead of 315 eV to eliminate the possible concern on scattered light. Qualitatively the intensity hence unoccupied density of state variation between samples follows the same trend as in (a).

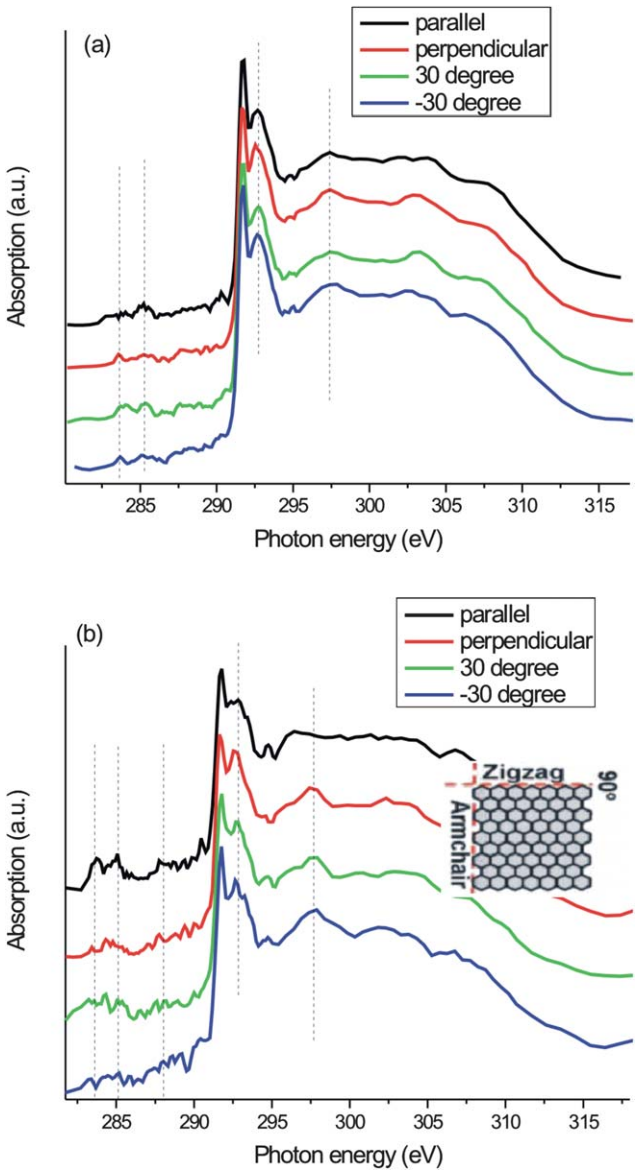

Fig. 6 C K-edge XANES of r-GO in regions 1 and 2 with different linear ***E*** vector orientations: (a) at the center (region 2) and (b) at the edge (region 1); the illustration of two types of edges, armchair *versus* zigzag is shown in the inset.

reflect that the sheet terminates at the edge (region 1). Since there is no azimuthal dependence for the intensity ratio of those two σ* resonances (molecular axis lies along the C–C bond) for any symmetry higher than 2 fold,[26] the armchair (2 C atoms per six member ring with a symmetry of 2 fold) should show a stronger σ* polarization difference with parallel and horizontal ***E*** vector relative to the edge (region 1) than that of the zigzag configuration (1 C atom per 6 member ring with infinity symmetry), although at present we do not have sufficient spatial resolution to unambiguously distinguish between the termination configuration, armchair and zigzag in region 1. It is also noted that the 1st σ* (291.7 eV) is more angle sensitive than 2nd σ* (292.7 eV) in both regions. The angle dependent information clearly shows the structural variation between the edge and the center of this particular r-GO sheet though further investigations are needed to find out the origin of these experimental observations.

Table 2 Normalized 1st and 2nd σ* resonances with different azimuthal linear polarization angles for the edge and center regions of the single r-GO sheet as noted in Fig. 7

	Normalized intensity			
	Edge		Center	
Polarization angle	1st σ* (exciton)	2nd σ*	1st σ* (exciton)	2nd σ*
Parallel	5.58	4.49	5.63	4.38
Perpendicular	4.61	4.12	5.13	4.32
30 degree	4.44	4.28	5.53	4.69
−30 degree	5.00	4.14	5.54	4.50

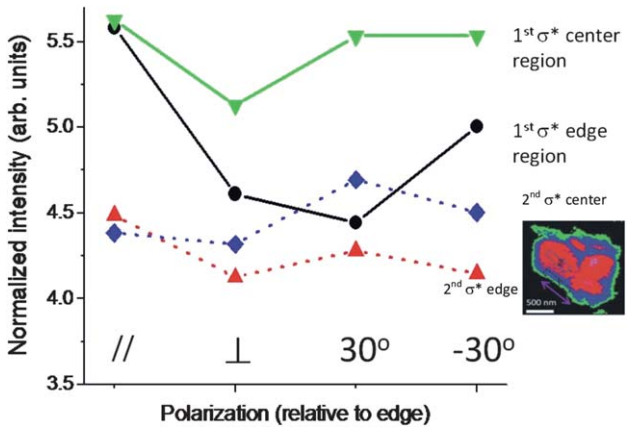

Fig. 7 Azimuthal linear polarization dependence of the σ* resonance in the single multilayer r-GO sheet. The orientation of the polarization parallel to the edge is illustrated in the inset.

4. Conclusions

We have reported the chemical mapping of a single r-GO sheet using XANES obtained by STXM with a spatial resolution of 30 nm. The analysis of STXM at the C K-edge clearly reveals the layered structure in a single sheet of r-GO and the edge in each layer. We have been able to track the number of layers by observing the discrete increment of the optical density. Variations in the electronic structure and bonding between edge and center locations have also been studied. The unusually sharp σ* resonance is observed in the thin r-GO layer and is attributed in part to the presence of non-graphitic domains and much reduced interaction between r-GO layers if any, consequently, a very localized transition. The azimuthal dependence of C K-edge XANES on the linear polarization of the incoming photon observed at the edge and the center regions shows that there exists more significant angle dependence in the edge of the graphene due to broken symmetry. The r-GO sample was also characterized by TEM, AFM and Raman spectroscopy which strongly support the STXM results.

Acknowledgements

The Canadian Light Source is supported by the Natural Sciences and Engineering Research Council of Canada, the National Research Council Canada, the Canadian Institutes of Health Research, the Province of Saskatchewan, Western Economic Diversification Canada, and the University of Saskatchewan. Raman spectroscopy and AFM measurements were completed at the Saskatchewan Structural Sciences Centre, which is supported by the University of Saskatchewan. The author (W.F.P.) acknowledges the National Science Council of Taiwan for financial support under NSC99-2119-M032-004-MY3.Research at the University of Western Ontario is supported by NSERC , CFI, CRC and OIT.

References

1 K. S. Novoselov, A. K. Geim, S. V. Morozov, D. Jiang, Y. Zhang, S. V. Dubonos, I. V. Grigorieva and A. A. Firsov, *Science*, 2004, **306**, 666.
2 A. K. Geim, *Science*, 2009, **324**, 1530.
3 A. K. Geim and K. S. Novoselov, *Nat. Mater.*, 2007, **6**, 183.
4 C. Lee, X. D. Wei, J. W. Kysar and J. Hone, *Science*, 2008, **321**, 385.
5 V. Lee, C. Park, C. Jaye, D. A. Fischer, Q. K. Yu, W. Wu, Z. H. Liu, S. S. Pei, C. Smith, P. Lysaght and S. Banerjee, *J. Phys. Chem. Lett.*, 2010, **1**, 1247.
6 H. L. Wang, J. T. Robinson, G. Diankov and H. J. Dai, *J. Am. Chem. Soc.*, 2010, **132**, 3270.
7 S. Park and R. S. Ruoff, *Nat. Nanotechnol.*, 2009, **4**, 217.
8 H. K. Jeong, H. J. Noh, J. Y. Kim, M. H. Jin, C. Y. Park and Y. H. Lee, *Europhys. Lett.*, 2008, **82**, 67004.
9 X. L. Li, H. L. Wang, J. T. Robinson, H. Sanchez, G. Diankov and H. J. Dai, *J. Am. Chem. Soc.*, 2009, **131**, 15939.
10 H. L. Wang, L. F. Cui, Y. A. Yang, H. S. Casalongue, J. T. Robinson, Y. Y. Liang, Y. Cui and H. J. Dai, *J. Am. Chem. Soc.*, 2010, **132**, 13978.
11 V. Lee, L. Whittaker, C. Jaye, K. M. Baroudi, D. A. Fischer and S. Banerjee, *Chem. Mater.*, 2009, **21**, 3905.
12 H. L. Wang, H. S. Casalongue, Y. Y. Liang and H. J. Dai, *J. Am. Chem. Soc.*, 2010, **132**, 7472.
13 Y. Y. Liang, H. L. Wang, H. S. Casalongue, Z. Chen and H. J. Dai, *Nano Res.*, 2010, **3**, 701.
14 X. R. Wang, X. L. Li, L. Zhang, Y. Yoon, P. K. Weber, H. L. Wang, J. Guo and H. J. Dai, *Science*, 2009, **324**, 768.
15 R. K. Joshi, H. Gomez, F. Alvi and A. Kumar, *J. Phys. Chem. C*, 2010, **114**, 6610.
16 J. G. Zhou, X. T. Zhou, X. H. Sun, R. Y. Li, M. Murphy, Z. F. Ding, X. L. Sun and T. K. Sham, *Chem. Phys. Lett.*, 2007, **437**, 229.
17 J. Zhou, J. Wang, H. Fang, C. Wu, J. N. Cutler and T. K. Sham, *Chem. Commun.*, 2010, **46**, 2778.
18 J. G. Zhou, H. T. Fang, Y. F. Hu, T. K. Sham, C. X. Wu, M. Liu and F. Li, *J. Phys. Chem. C*, 2009, **113**, 10747.
19 J. G. Zhou, H. T. Fang, J. M. Maley, J. Y. P. Ko, M. Murphy, Y. Chu, R. Sammynaiken and T. K. Sham, *J. Phys. Chem. C*, 2009, **113**, 6114.
20 N. L. Yang, J. Zhai, D. Wang, Y. S. Chen and L. Jiang, *ACS Nano*, 2010, **4**, 887.
21 J. G. Zhou, H. T. Fang, J. M. Maley, M. W. Murphy, J. Y. P. Ko, J. N. Cutler, R. Sammynaiken, T. K. Sham, M. Liu and F. Li, *J. Mater. Chem.*, 2009, **19**, 6804.
22 J. G. Zhou, X. T. Zhou, R. Y. Li, X. L. Sun, Z. F. Ding, J. Cutler and T. K. Sham, *Chem. Phys. Lett.*, 2009, **474**, 320.
23 J. G. Zhou, X. T. Zhou, X. H. Sun, M. Murphy, F. Heigl, T. K. Sham and Z. F. Ding, *Can. J. Chem.*, 2007, **85**, 756.
24 A. Felten, C. Bittencourt, J. J. Pireaux, M. Reichelt, J. Mayer, D. Hernandez-Cruz and A. P. Hitchcock, *Nano Lett.*, 2007, **7**, 2435.
25 A. Felten, H. Hody, C. Bittencourt, J. J. Pireaux, D. H. Cruz and A. P. Hitchcock, *Appl. Phys. Lett.*, 2006, **89**, 093123-1.
26 J. Stöhr, *NEXAFS Spectroscopy*, Springer-Verlag, Berlin, 1992.
27 V. M. Pereira, F. Guinea, J. dos Santos, N. M. R. Peres and A. H. C. Neto, *Phys. Rev. Lett.*, 2006, **96**, 4.
28 T. K. Sham, *Int. J. Nanotechnol.*, 2008, **5**, 1194.
29 K. V. Kaznatcheev, C. Karunakaran, U. D. Lanke, S. G. Urquhart, M. Obst and A. P. Hitchcock, *Nucl. Instrum. Methods Phys. Res., Sect. A*, 2007, **582**, 96.
30 D. W. Lee, L. De Los Santos, J. W. Seo, L. L. Felix, A. Bustamante, J. M. Cole and C. H. W. Barnes, *J. Phys. Chem. B*, 2010, **114**, 5723.
31 M. Weser, Y. Rehder, K. Horn, M. Sicot, M. Fonin, A. B. Preobrajenski, E. N. Voloshina, E. Goering and Y. S. Dedkov, *Appl. Phys. Lett.*, 2010, **96**, 012504-1.
32 O. Wessely, M. I. Katsnelson, A. Nilsson, A. Nikitin, H. Ogasawara, M. Odelius, B. Sanyal and O. Eriksson, *Phys. Rev. B: Condens. Matter Mater. Phys.*, 2007, **76**, 161402.
33 W. J. Hua, B. Gao, S. H. Li, H. Agren and Y. Luo, *Phys. Rev. B: Condens. Matter Mater. Phys.*, 2010, **82**, 155433.
34 Z. T. He, X. M. Yang, H. H. Xia, X. T. Zhou and T. K. Sham, to be published.
35 J. G. Zhou, J. Wang, H. T. Fang and T. K. Sham, *J. Mater. Chem.*, 2011, **21**, 5944.
36 J. G. Zhou, J. Wang, H. Liu, M. N. Banis, X. L. Sun and T. K. Sham, *J. Phys. Chem. Lett.*, 2010, **1**, 1709.
37 W. S. Hummers and R. E. Offeman, *J. Am. Chem. Soc.*, 1958, **80**, 1339.
38 Y. Ma, C. T. Chen, G. Meigs, K. Randall and F. Sette, *Phys. Rev. A: At., Mol., Opt. Phys.*, 1991, **44**, 1848.

39 A. C. Ferrari, J. C. Meyer, V. Scardaci, C. Casiraghi, M. Lazzeri, F. Mauri, S. Piscanec, D. Jiang, K. S. Novoselov, S. Roth and A. K. Geim, *Phys. Rev. Lett.*, 2006, **97**, 4.
40 D. Graf, F. Molitor, K. Ensslin, C. Stampfer, A. Jungen, C. Hierold and L. Wirtz, *Nano Lett.*, 2007, **7**, 238.
41 E. Najafi, D. H. Cruz, M. Obst, A. P. Hitchcock, B. Douhard, J. J. Pireaux and A. Felten, *Small*, 2008, **4**, 2279.
42 M. H. Gass, U. Bangert, A. L. Bleloch, P. Wang, R. R. Nair and A. K. Geim, *Nat. Nanotechnol.*, 2008, **3**, 676.
43 A. A. Green and M. C. Hersam, *Nano Lett.*, 2009, **9**, 4031.
44 L. Y. Jiao, L. Zhang, X. R. Wang, G. Diankov and H. J. Dai, *Nature*, 2009, **458**, 877.
45 D. Pacile, M. Papagno, A. F. Rodriguez, M. Grioni and L. Papagno, *Phys. Rev. Lett.*, 2008, **101**, 066806.
46 F. Tuinstra and J. L. Koenig, *J. Chem. Phys.*, 1970, **53**, 1126.
47 J. W. Chiou, C. L. Yueh, J. C. Jan, H. M. Tsai, W. F. Pong, I. H. Hong, R. Klauser, M. H. Tsai, Y. K. Chang, Y. Y. Chen, C. T. Wu, K. H. Chen, S. L. Wei, C. Y. Wen, L. C. Chen and T. J. Chuang, *Appl. Phys. Lett.*, 2002, **81**, 4189.

